Roughening and strain-field evolution at a grain boundary in α-Al_2O_3

Sung Bo Lee,[1,*] Seung-Yong Lee,[1] Seung Jo Yoo,[2] Yoonkoo Kim,[1] Jin-Gyu Kim,[2] Miyoung Kim,[1] and Heung Nam Han[1]

[1]*Department of Materials Science and Engineering and Research Institute of Advanced Materials (RIAM), Seoul National University, Seoul 08826, South Korea*

[2]*Electron Microscopy Research Center, Korea Basic Science Institute (KBSI), Daejeon 34133, South Korea*

(Received 5 July 2018; revised manuscript received 29 September 2018; published 29 November 2018)

Using a combination of high-resolution transmission electron microscopy (HRTEM), geometric phase analysis of HRTEM images, and scanning TEM, we study the structural transition and strain-field evolution at the grain boundary in an α-Al_2O_3 bicrystal with a misorientation relationship of $[0\,0\,0\,1]/30^\circ$. The specimens are annealed at 300, 500, and 700 °C in the TEM. The grain boundaries in the specimens before annealing and annealed at 300 °C are observed to be faceted, but the grain boundaries in those annealed at 500 and 700 °C become defaceted, exhibiting meandering morphology. Interestingly, for the as-received specimen and that annealed at 300 °C, there occurs a periodic strain fluctuation along the grain boundary. However, such a periodic fluctuation along the grain boundary is not observed in the specimens annealed at 500 and 700 °C. These results suggest an unexplored possibility that the roughening transition of a grain boundary is enhanced by strain relaxation occurring at the grain boundary.

DOI: 10.1103/PhysRevMaterials.2.113405

I. INTRODUCTION

Grain boundaries (GB) control many important properties (e.g., mechanical, electrical, and nuclear) of crystalline materials and thus a detailed characterization of the GB structure at the atomic level is crucial for thermomechanical processing to produce desirable materials properties. Thermomechanical processing techniques involve thermally activated GB migration.

As is well evidenced, crystalline surfaces undergo thermal roughening transitions [1–5] for simple thermodynamic reasons: Above a critical temperature, the free energy required to form a step on a crystalline terrace surface (step free energy) goes to zero. The thermal roughening transition corresponds to the disappearance of cusps in the polar plot of the surface free energy with respect to the surface-normal direction [6], which is accompanied by faceting–defaceting transitions at orientations near the cusp ones [6,7]. Even below the thermal roughening transition temperatures, crystalline surfaces can be roughened with increasing driving force for migration because steps on the surface lose their identity with increasing driving force for migration, the step free energy becoming zero [8–12]. This is defined as kinetic roughening.

Likewise, such transitions hold for grain boundaries. The GB thermal roughening transition of a cusp GB plane orientation is accompanied by defaceting transitions of orientations near the cusp one [13,14]. The GB faceting–defaceting transition occurs with temperature increasing or with the introduction/removal of impurities [14–25].

Kinetic roughening of GBs is revealed by transmission electron microscopy (TEM) studies using bicrystals of $SrTiO_3$ [26], ZnO [27], and GaN [28,29], where the GB was driven to migrate by the difference in surface energy between two grains meeting at the GB and its magnitude was controlled by the specimen thickness. The GBs underwent a shape change from atomically stepped to undulating with increasing the driving force for migration even well below the thermal roughening transition temperatures, exhibiting a sign of kinetic roughening. It is accepted that flat and singular GBs corresponding to cusp orientations migrate by a step mechanism and rough ones advance by a continuous mechanism [26–29]. As such, the GB structure and migration mechanism is affected by the GB roughening transition, and thus knowledge of the GB roughening transition at the atomic level is of great importance.

The aforementioned results show that GB roughening transitions are a function of temperature [13,14,19,21,22], solute [15–19,23,24], and driving force for migration [26–29]. However, GBs necessarily contain strain originating from misfit localization and distortion of the lattice at and near to the GBs. Actually, Merkle and his colleagues [30,31] identified such structural modulations by contrast effects shown in high-resolution TEM (HRTEM) images of twist and general GBs in Au. However, the correlation between strain stored at GBs and the roughening transition has been out of research interests.

In the present paper we suggest that, besides the above effects, the GB roughening transition can be induced by elastic strain developing at GBs. In this study we have used an α-Al_2O_3 bicrystalline GB composed of $[1\ -1\ 0\ 0]$- and $[1\ -2\ 1\ 0]$-oriented grains and annealed it in a TEM at 300, 500, and 700 °C. The initial GB and that annealed at 300 °C reveal faceted structure, and intriguingly, a cycle of tensile-compressive strains appears at the GB. However, at the higher temperatures of 500 and 700 °C, the GB is roughened and no periodic strain fluctuation appears. Our study demonstrates that the GB roughening is partly attributed to the phenomenon of the strain effect.

*bolee@snu.ac.kr

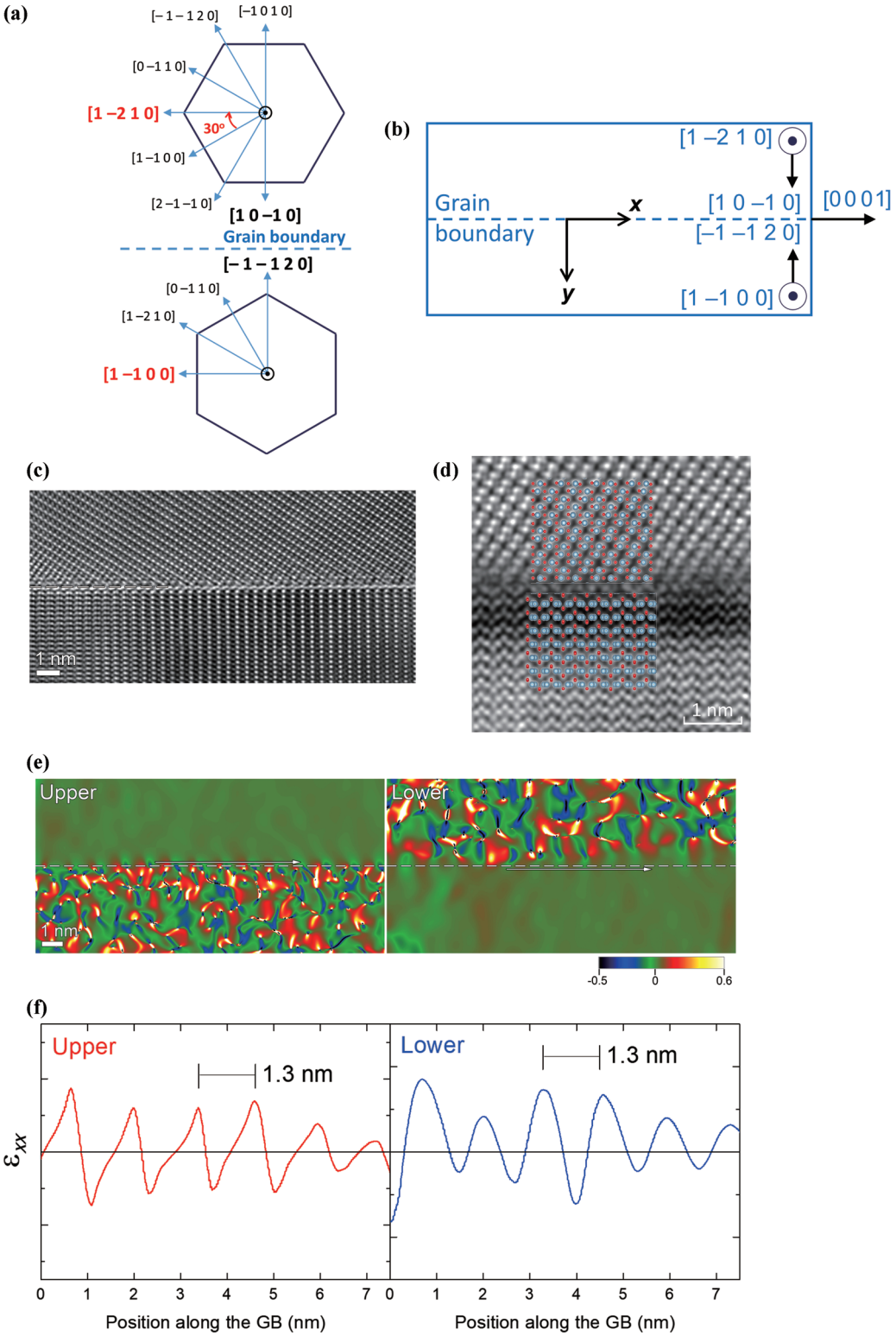

FIG. 1. (a) Schematic diagram of the bicrystal projected along the [0 0 0 1] direction. If the upper grain is rotated about [0 0 0 1] by 30°, the lower one is obtained. The GB is bounded by (1 0 −1 0) and (−1 −1 2 0) (highlighted in bold). (b) Crystallographic directions of FIB specimens extracted from the GB area in the α-Al_2O_3 bicrystal. (c) HRTEM image showing the as-received state of a GB bounded by (−1 −1 2 0) and (1 0 −1 0) planes of two grains with surface normal directions of [1 −1 0 0] and [1 −2 1 0], respectively. (d) HAADF-STEM image of the GB with an overlay of a structure model (blue for aluminum and red for oxygen). The image was filtered for noise reduction. (e) Strain maps of ε_{xx} corresponding to the HRTEM image shown in (c) with respect to the upper and lower grains (left and right panels, respectively). The x and y directions are chosen to be parallel and normal to the GB, respectively. The color bar indicates the full strain range from −0.5 to 0.6. (f) The strain fields of ε_{xx} with respect to the upper and lower grains are also represented along the GB [indicated by white arrows in (e)] as line profiles.

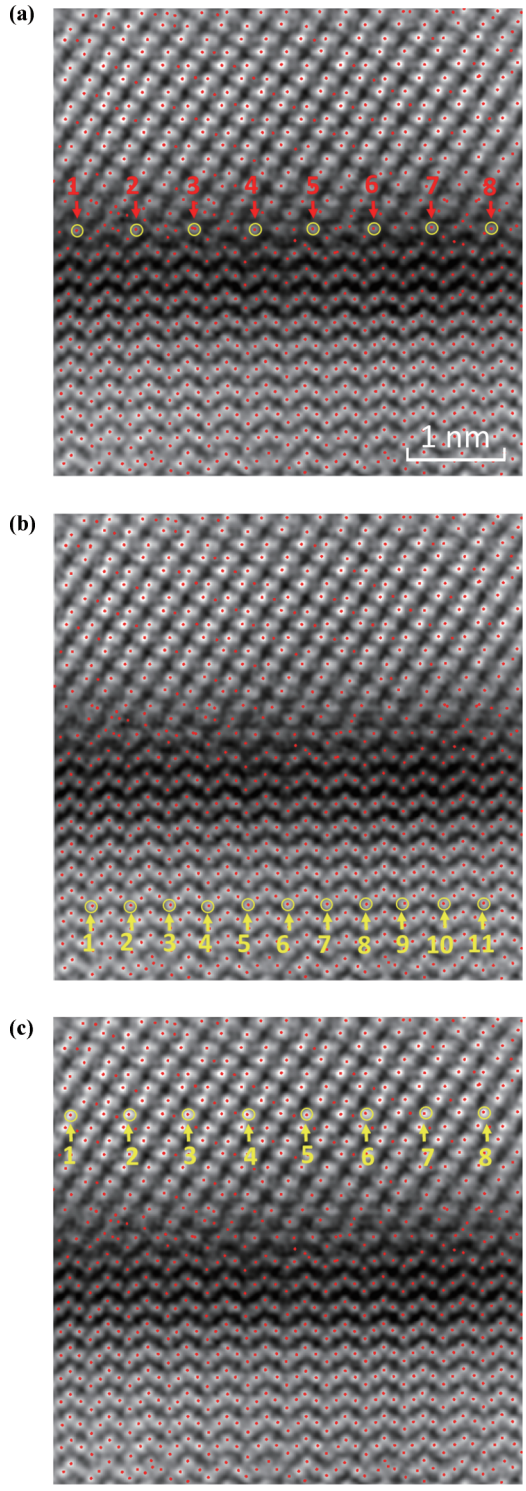

FIG. 2. Determination of atom positions in the HRSTEM image of Fig. 1(d) determined by two-dimensional quadratic fitting functions. (a) Selection of atom positions along the GB. (b) Selection of atom positions far from the GB in the lower grain side. (c) Selection of atom positions far from the GB in the upper grain side.

II. EXPERIMENTAL

An α-Al_2O_3 (trigonal; space group: $R\bar{3}c$) bicrystal (Shinkosha Co., Ltd., Japan) was used for the experiment. The bicrystalline GB had a misorientation relationship of [0 0 0 1]/30° with a *tilt* characteristic with an asymmetric GB plane [bounded by (1 0 −1 0) and (−1 −1 2 0) planes] [Fig. 1(a)]. TEM specimens were prepared by focused ion-beam (FIB) lift-out technique from the bicrystal surface with the surface-normal directions of [0 0 0 1] [Fig. 1(a)] with the GB passing through the center of the specimens. The cross-section lamellae specimens for HRTEM were prepared on a FIB workstation (FEI Nova 200 Nanolab dual-beam FIB). The specimens were thus composed of two grains with different surface-normal directions of [1 −2 1 0] [upper grain, Fig. 1(b)] and [1 −1 0 0] [lower grain, Fig. 1(b)]. The prepared specimens were heated with the electron beam *off* to 300 and 500 °C at a heating rate of 20 °C/min in a high-voltage TEM (HVTEM) operating at 1250 keV (0.12-nm point-to-point resolution) (JEOL JEM-ARM1300S), which is equipped with a side-entry heating stage. The base pressure in the specimen chamber of the HVTEM was $\sim 2 \times 10^{-6}$ Pa. Annealings were done at 300 °C for 5 h, at 500 °C for 2 h, and at 700 °C for 30 min with the beam still off. All observations were made after cooling to room temperature to avoid the possible knock-on damage during *in situ* observations at the high temperatures. According to Pells and Phillips [32,33], the displacement energies of Al and O atoms in α-Al_2O_3 are 18 and 75 eV, respectively. These values correspond to the threshold energies for displacement [34] of 187 keV for Al and 395 keV for O, which are lower than the incident energy of 1250 keV. Thus, knock-on damage by high-energy electrons is not negligible with increasing temperature [33,34]. Actually, α-Al_2O_3 tends to dissociate at elevated temperatures under electron-beam illumination at 1250 keV [35]. This is the reason why we chose *ex situ* observations. The thickness of the specimens was measured by electron-energy-loss spectroscopy log-ratio method [36] in the HVTEM.

Quantitative measurements of local strain components at the GB were carried out by geometric phase analysis (GPA) [37]. The method is based upon selecting a particular set of strong noncollinear reflections in the Fourier transform of an HRTEM lattice image (for two-dimensional displacement/strain fields) and performing an inverse Fourier transform. Comparing it with the reference image obtained at a perfect crystalline region extracts a two-dimensional displacement vector field, whose derivative then produces local strain components. The reference area is independently defined within each grain of the bicrystal specimen. In the present study the spatial resolution of the analysis was 1 nm with a measurement precision of ∼0.1%. To remove strain artifact induced by projection lens distortions in the microscope, the GPA processes were calibrated by reference mapping of local displacement field variation in the HRTEM image of an unstrained, perfect crystalline Au standard sample [38].

Atomic-resolution high-angle annular dark-field–scanning TEM (HAADF-STEM) images were acquired by a spherical aberration (Cs)-corrected (probe corrector) TEM instrument with a cold-field emission gun operated at 200-keV acceleration voltage (ARM-200CF, JEOL), which is installed at the National Center for Inter-University Research Facilities at Seoul National University. The STEM images were obtained under probe convergence semiangle of ∼25 mrad,

TABLE I. Spacing values obtained from Fig. 2(a).

Point-point	1–2	2–3	3–4	4–5	5–6	6–7	7–8
Spacing (nm)	0.6201	0.5913	0.6516	0.6059	0.6357	0.6069	0.6251

acceptance semiangle between 90 and 370 mrad, and 23-pA probe current.

III. RESULTS

In the as-received state, the GB is atomically flat, as shown in Fig. 1(c). A high-resolution STEM (HRSTEM) image [Fig. 1(d)] shows that the Al(0 0 0 1) plane and the O(0 0 0 1) plane of the one grain are matched to the O(0 0 0 1) plane and the Al(0 0 0 1) plane of the other grain, respectively, across the GB. Figure 1(e) maps in-plane strain fields (ε_{xx}) near and at the GB with respect to the upper and lower grains (left and right panels, respectively). Interestingly, there exists along the GB a strain fluctuation with a periodicity of ∼1.3 nm [also see a line profile of Fig. 1(f)], although there is a coherence in the common [0 0 0 1] direction (designated as $\boldsymbol{x}$) [Fig. 1(b)]. For the maps with respect to the upper grain (left panel), the region below the GB (indicated by a dashed line) is not relevant, because it has no phase relation with the upper grain and just shows featureless noise. For the maps with respect to the lower grain, conversely, the region below the GB will not be relevant, because it has no phase relation with the upper grain.

The periodic fluctuation in ε_{xx} shown by GPA [Figs. 1(e) and 1(f)] is confirmed by analysis results of atom positions in the HRSTEM image of Fig. 1(d) determined by two-dimensional quadratic fitting functions [39,40] [Figs. 2(a)–2(c); Tables I–III; see Supplemental Material [40] for details of its method]. After determining atom positions in Fig. 1(d), then we measured the spacing between atom positions aligned along the GB, as shown in Fig. 2(a). The spacing between peaks 1–3 (equivalently, 2–4, 3–5, etc.) corresponds to the interplanar spacing of (0 0 0 1). Very interestingly, the interatomic spacing (1–2, 2–3, 3–4, etc.) is not equidistant, but alternately enlarging and shortening at ∼30-pm level along the GB [Fig. 2(a), Table I]. On the other hand, the spacing between atoms far from the GB remains nearly equidistant [Fig. 2(b), Table II; Fig. 2(c), Table III]. The spacing values have a very high accuracy with an error of ∼10-pm level. These results indicate that there occurs a strain fluctuation along the GB with a periodicity of the interplanar spacing of (0 0 0 1), which is in agreement with the GPA result [Figs. 1(e) and 1(f)].

As for the initial state [Fig. 1(c)], after annealing at 300 °C the GB is observed to be atomically flat, intermittently separated by atomic-scale facets, as shown in Fig. 3(a). Also for the GB annealed at 300 °C, the strain fields of ε_{xx} with respect to the upper and lower grains (left and right panels, respectively) fluctuate along the GB with the same periodicity as for the initial state [Figs. 3(b) and 3(c)].

At higher temperatures at 500 and 700 °C, the GB becomes rough with wavy morphology [Figs. 4(a), 4(b), and 5(a)]. After annealing at 500 °C, the GB became roughened with wavy morphology [Fig. 4(a)]. As shown in Fig. 4(a), moiré patterns are formed due to overlapping of the two grains meeting at the GB, leaving behind a trace of the original GB position, as indicated by a dashed line. At a different GB region, the GB is observed to become fully curved [Fig. 4(b)]. In the GB annealed at 700 °C, the GB is also observed to be rough, as shown in Fig. 5(a). At 700 °C, facet structures seem to remain. This is probably due to the short annealing time at the temperature. Regrettably, longer annealing times at the temperature tend to make the specimen warped. If annealed further, the GB would be expected to be completely wavy and rough, as observed at 500 °C. As shown in Figs. 4(c), 4(d), 5(b), and 5(c), the GB after annealing at 500 and 700 °C does not exhibit any periodicity of strain fluctuation along the common [0 0 0 1] direction [indicated by white arrows in Figs. 4(c) and 5(b)]. Of course there is a strain field along the wavy GB observed, but, as noted before, it does not show any periodicity along the [0 0 0 1] direction. We have noted the disappearance of the periodicity at the higher temperatures, which is a major point of the present study.

IV. DISCUSSION

There is a coherence in the common [0 0 0 1] direction (designated as $\boldsymbol{x}$) [Fig. 1(b)]. However, in the $\boldsymbol{z}$ direction (parallel to [1 −2 1 0] for the upper grain and, equivalently, to [1 −1 0 0] for the lower grain), the GB is fully incoherent. Therefore, the elastic coherency strain along the $\boldsymbol{z}$ direction is neglected. We consider the common [0 0 0 1] direction for the possible elastic coherency strain. Theoretically there is no lattice misfit between the two lattices along the [0 0 0 1] direction, but interestingly there is a kind of coherency strain occurring at the GB. This is the main observation of the present study.

Presently, it is not straightforward why the tensile and compressive strains alternate in the periodicity of the interplanar spacing of (0 0 0 1) in the common [0 0 0 1] direction [Figs. 1(e), 1(f), 2(a), 3(b), and 3(c)]. However, the atomic structure models overlaid on the HRSTEM image [Fig. 1(d)] would be helpful. If we extend the structure models in both grains to meet each other at the GB (Fig. 6), a structural unit

TABLE II. Spacing values obtained from Fig. 2(b).

Point–point	1–2	2–3	3–4	4–5	5–6	6–7	7–8	8–9	9–10	10–11
Spacing (nm)	0.4018	0.4161	0.4016	0.4120	0.4116	0.4157	0.4112	0.4012	0.4044	0.4219

TABLE III. Spacing values obtained from Fig. 2(c).

Point-point	1–2	2–3	3–4	4–5	5–6	6–7	7–8
Spacing (nm)	0.6081	0.6163	0.6206	0.6215	0.6157	0.6134	0.6187

with the same atomic environment (indicated by blue circles) repeats itself along the GB at an interval of the interplanar spacing of (0 0 0 1) (∼1.3 nm). We relate the periodicity to the origin of periodic strain fluctuation shown in Figs. 1(e), 1(f), 2(a), 3(b), and 3(c). It is deduced that the periodic strain contrast is due to the localized structure with the same atomic environment which appears along the GB. The periodic strain fluctuation at the GB is taken to be a sign of coherency strain. Although there were reports [30,31] that periodic misfit localizations are observed in atomically *faceted* GBs, those associated with local strain along *flat coherent* GBs were not been identified.

The wavy morphology of the GB occurs by the increase in temperature from 300 to 500 °C and thus it appears that the morphological change is thermally activated, i.e., induced by thermal roughening transition. In addition to the thermal effect, the disappearance of periodicity in the fluctuation in ε_{xx} at the higher temperatures [Figs. 4(c), 4(d), 5(b), and 5(c)] certainly indicates that the observed roughening is partly due to the strain effect. Our experimental results suggest that the thermal roughening transition temperature critically depends on strains developed at a GB, which awaits further study.

Since the surface-normal directions of the two grains meeting at the GB are different, the surface-energy

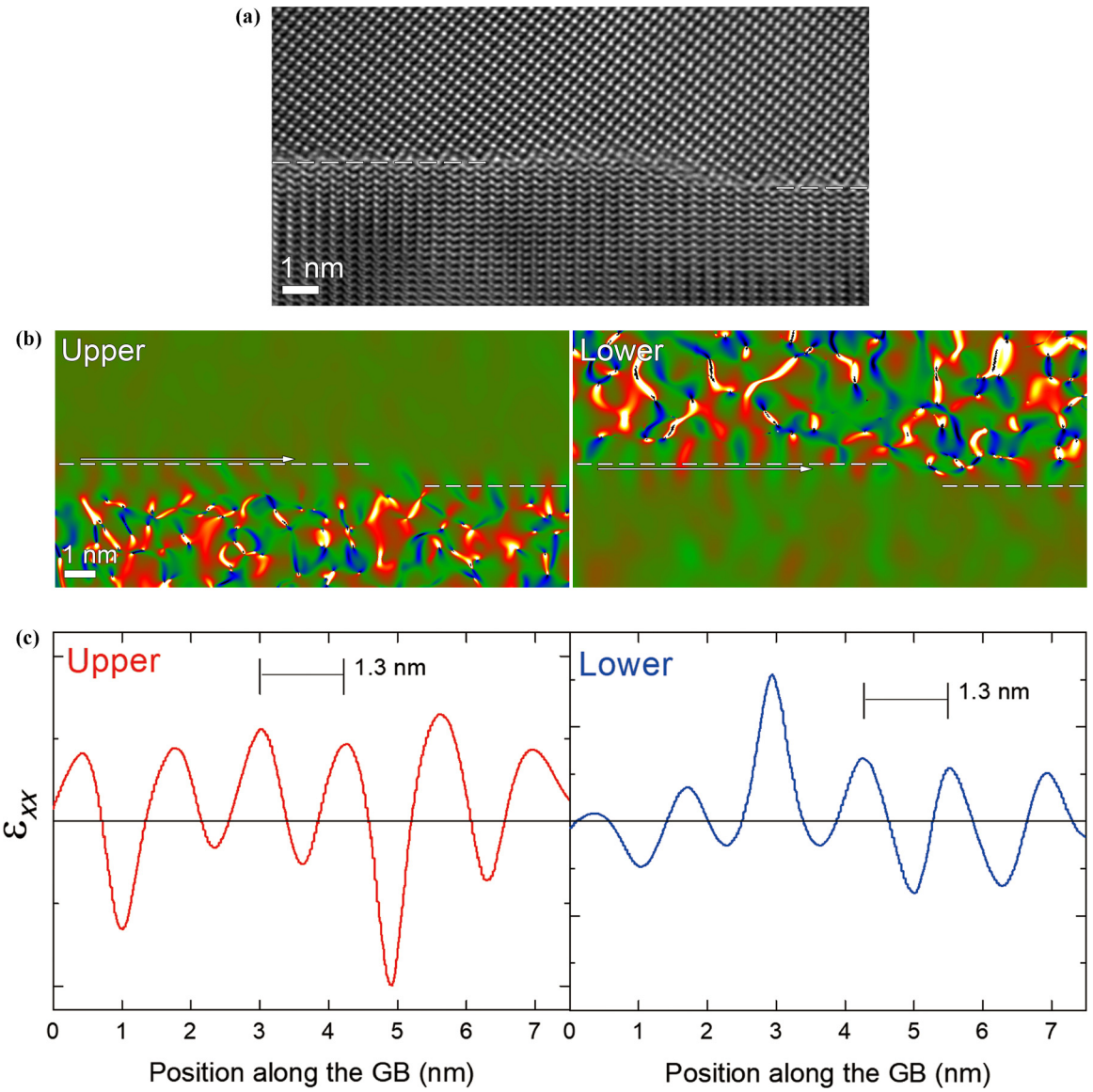

FIG. 3. (a) HRTEM image of the GB annealed at 300 °C. (b) Corresponding strain maps of ε_{xx} with respect to the upper and lower grains (left and right panels, respectively). (c) Line profiles of ε_{xx} along the GB.

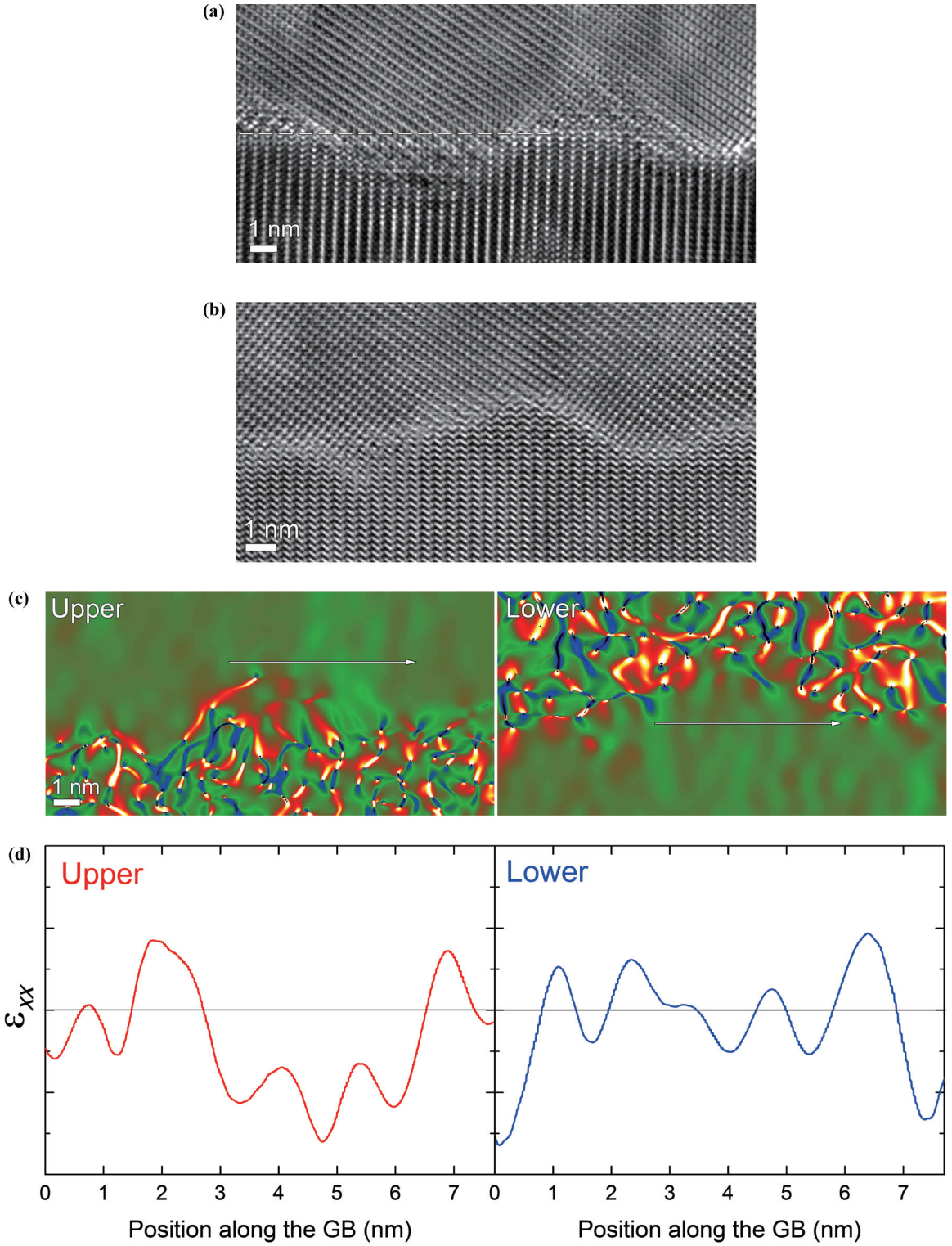

FIG. 4. (a), (b) HRTEM images of the GB annealed at 500 °C for 2 h. (c) Strain maps of ε_{xx} corresponding to (b) with respect to the upper and lower grains (left and right panels, respectively). (d) Line profiles of ε_{xx} near the GB. (In this case, the GB is wavy) and, for convenience's sake, we obtain profiles from straight lines near the GB [indicated by arrows shown in (c)] parallel to the $(-1\ -1\ 2\ 0)$ plane for the lower grain and the $(1\ 0\ -1\ 0)$ plane for the upper grain.

difference may provide a driving force for migration. Mackrodt *et al.* [41] calculated by the shell model the energies and relaxed structures of low-index surfaces in α-Al_2O_3. As a result, it was estimated that the surface energy of the relaxed $(1\ 0\ -1\ 0)$ surface ($2.23\,J\,m^{-2}$) is lower than that of the relaxed $(1\ 1\ -2\ 0)$ surface ($2.5\,J\,m^{-2}$). Manassidis and Gillan [40] also predicted a similar tendency by using the density-functional theory [$1.4\,J\,m^{-2}$ for $(1\ 0\ -1\ 0)$; $1.86\,J\,m^{-2}$ for

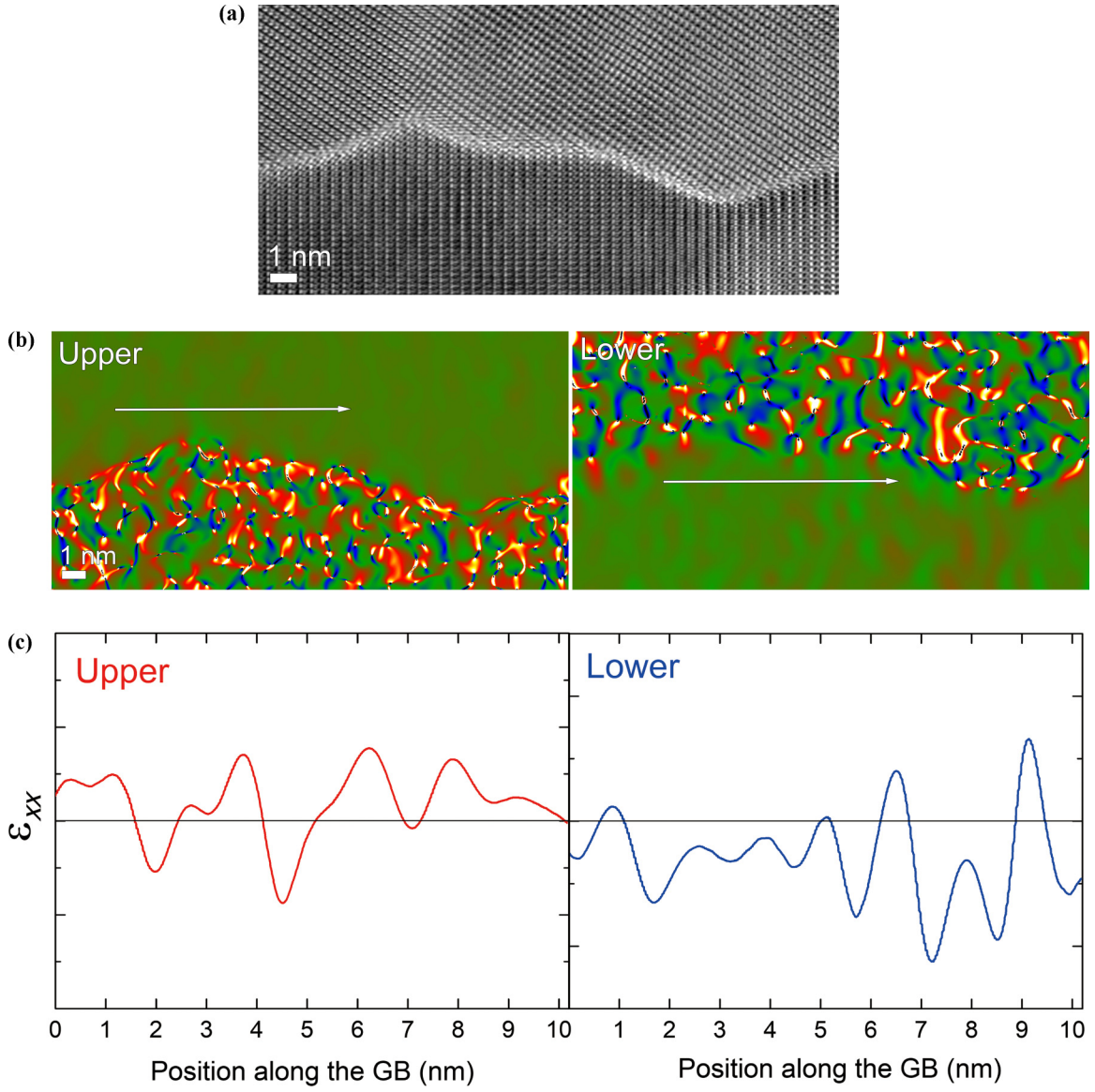

FIG. 5. (a) HRTEM image of the GB annealed at 700 °C. (b) Corresponding strain maps of ε_{xx} with respect to the upper and lower grains (left and right panels, respectively). (c) Line profiles of ε_{xx} near the GB.

(1 1 −2 0)]. However, somewhat contradictory to these results [41,42], Sun *et al.* [43] calculated by the periodic Hatree−Fock model that the surface energy of {1 0 −1 0} is even slightly larger than that of {1 1 −2 0} (2.44 vs 2.39 J m^{-2}).

Regardless of which grain has the lower surface energy, however, our experimental results obtained after annealing at 500 and 700 °C [Figs. 4(a), 4(b), and 5(a)] certainly appears to suggest that that there is no surface-energy anisotropy acting for GB migration in the present study. The moiré patterns marking a trace of the original GB position [Fig. 4(a)] indicate that the GB, initially flat, migrates to either grain, showing a zigzagged shape. That is, Fig. 4(a) clearly shows that the GB migrates not in one direction, but to either grain side from its original position. If the GB migration was caused by the surface-energy anisotropy, the GB would migrate in one direction according to the surface-energy anisotropy, in contrast to the observation. It is thus presumed that the surface-energy anisotropy may disappear due to the entropy associated with the respective surfaces at the high temperatures used in the present study. Although the present observations could not capture the GB migration *in situ*, the moiré patterns observed at 500 °C [Fig. 4(a)] fully clarify that the GB migration in the present study is not driven by the surface-energy anisotropy.

As noted above, the surface-energy anisotropy does not seem to act as a driving force for migration. Moreover, the zigzagged GB migration [Fig. 4(a)] even indicates that no definite driving force for GB migration exists. If the roughening transition (Figs. 4 and 5) was caused by kinetic roughening, the kinetically roughened GB would migrate in one direction according to the surface-energy anisotropy, which is in contrast to the observation. Thus we can discard the possibility of kinetic roughening as a reason for the morphological change.

The fact that the roughening at 500 and 700 °C [Figs. 4(a), 4(b), and 5(a)] is accompanied by the disappearance of periodicity in the fluctuation in ε_{xx} [Figs. 4(c), 4(d), 5(b), and

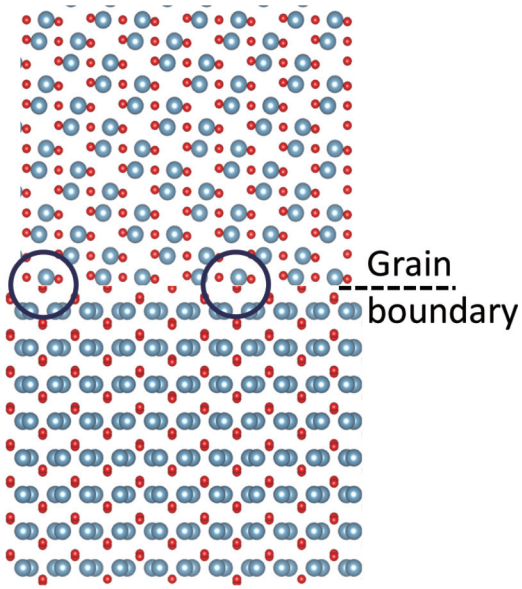

FIG. 6. Extension the atomic structure models overlaid on the HRSTEM image [Fig. 1(d)] in both grains to meet each other at the GB.

5(c)] seems to certainly indicate that the thermal roughening transition is enhanced by a decrease in the strain energy stored at the GB. These results strongly demonstrate that the coherency strain at the GB begins to disappear at the high temperatures. For a crystalline surface, according to Asaro and Tiller [44] and Grinfeld [45], the elastic strain energy stored at a flat surface is released by making it rough with wavy morphology, which balances the increase in surface energy. It was observed that misfit strain can cause the film surface to be roughened without any introduction of dislocations, e.g., for Ge grown on Si(100) [46] and for Si_xGe_{1-x} film grown on Si(100) [47]. We suggest that such an instability condition [44–47] holds for our GB case. As for the film surfaces, elastic strain may provide the driving force for GB roughening: The roughening transition proceeds at the expense of the strain energy stored at the GB while there is a gain in GB energy by increasing the GB area.

V. CONCLUDING REMARKS

To sum up, we could observe that the roughening transition of an α-Al_2O_3 bicrystalline GB occurs in conjunction with a disappearance of periodicity in the strain fluctuation along the GB. The observed transition occurs by a combination of thermal and strain effects. This work suggests that the thermal roughening of the GB can be enhanced by strain relaxation at the GB. It certainly appears that it is nothing to do with kinetic roughening. This is because the GB does not migrate in one direction according to the driving force for migration but fluctuates to either grain side from the original position at the high temperatures, exhibiting meandering morphology. The results of this study suggest that GB roughening can be induced by the strain relaxation occurring at the GB, as verified for the surfaces [46,47]. This study provides insights into understanding of the GB structure and its transition by revealing the strain effect on the GB roughening transition. Calculation work is in progress for the simulation of the periodic strain fluctuation. Furthermore, our study awaits development of atomistic modeling and simulation of the strain energy distribution at GBs for more detailed information on the strain effect on the GB roughening transition, which, we hope, will lead to the development of more comprehensive models of the roughening transition of GBs.

ACKNOWLEDGMENTS

One of the authors (S.B.L.) thanks Dr. Heejin Kim (Korea Basic Science Institute) for his valuable comments on the possible calculation study. We appreciate financial support from the Korea Basic Science Institute under the R&D program (Project No. D37700) supervised by the Ministry of Science and ICT. This research was also supported by the Basic Science Research Program through the National Research Foundation of Korea funded by the Ministry of Education (Grant No. 2016R1D1A1A09916302) (RIAM) and by the Engineering Research Center (ERC) program of the National Research Foundation of Korea funded by the Ministry of Science and ICT (Grant No. 2015R1A5A1037627).

[1] W. K. Burton, N. Cabrera, and F. C. Frank, Philos. Trans. R. Soc. London, Ser. A **243**, 299 (1951).
[2] S. T. Chui and J. D. Weeks, Phys. Rev. B **14**, 4978 (1976).
[3] H. van Beijeren, Phys. Rev. Lett. **38**, 993 (1977).
[4] J. E. Avron, L. S. Balfour, C. G. Kuper, J. Landau, S. G. Lipson, and L. S. Schulman, Phys. Rev. Lett. **45**, 814 (1980).
[5] P. E. Wolf, F. Gallet, S. Balibar, and E. Rolley, J. Phys. (Paris) **46**, 1987 (1985).
[6] C. Herring, Phys. Rev. **82**, 87 (1951).
[7] M. Wortis, in *Chemistry and Physics of Solid Surfaces VII*, edited by R. Vanselow and R. F. Howe (Springer, Berlin, 1988), Chap. 13.
[8] J. W. Cahn, Acta Metall. **8**, 554 (1960).
[9] G. H. Gilmer, J. Cryst. Growth **49**, 465 (1980).
[10] E. van Veenendaal, P. J. C. M. van Hoof, J. van Suchtelen, W. J. P. van Enckevort, and P. Bennema, Surf. Sci. **417**, 121 (1998).
[11] H. M. Cuppen, H. Meekes, W. J. P. van Enckevort, E. Vlieg, and H. J. F. Knops, Phys. Rev. B **69**, 245404 (2004).
[12] S. D. Peteves and R. Abbaschian, Metall. Mater. Trans. A **22A**, 1271 (1991).
[13] T. E. Hsieh and R. W. Balluffi, Acta Metall. **37**, 2133 (1989).
[14] S. B. Lee, W. Sigle, W. Kurtz, and M. Rühle, Acta Mater. **51**, 975 (2003).
[15] G. Henry, J. Plateau, X. Waché, M. M. Gerber, I. Behar, and C. Crussard, Mem. Sci. Rev. Metall. **56**, 417 (1959).
[16] C. Pichard, J. Rieu, and C. Goux, Mem. Sci. Rev. Metall. **70**, 13 (1973).
[17] A. M. Donald and L. M. Brown, Acta Metall. **27**, 59 (1979).
[18] T. G. Ference and R. W. Balluffi, Scr. Metall. **22**, 1929 (1988).
[19] S. B. Lee, N. M. Hwang, D. Y. Yoon, and M. F. Henry, Metall. Mater. Trans. A **31A**, 985 (2000).

[20] S. B. Lee, D. Y. Yoon, and M. F. Henry, Acta Mater. **48**, 3071 (2000).
[21] S. B. Lee, W. Sigle, and M. Rühle, Acta Mater. **51**, 4583 (2003).
[22] S. B. Lee, J.-H. Lee, P.-S. Cho, D.-Y. Kim, W. Sigle, and F. Phillipp, Adv. Mater. **19**, 391 (2007).
[23] B. K. Lee, S. Y. Chung, and S.-J. L. Kang, Acta Mater. **48**, 1575 (2000).
[24] Y. I. Jung, S. Y. Choi, and S.-J. L. Kang, Acta Mater. **54**, 2849 (2006).
[25] B. B. Straumal, O. A. Kogtenkova, A. S. Gornakova, V. G. Sursaeva, and B. Baretzky, J. Mater. Sci. **51**, 382 (2016).
[26] S. B. Lee and Y.-M. Kim, Acta Mater. **57**, 5264 (2009).
[27] S. B. Lee, Y.-M. Kim, D.-S. Ko, T.-Y. Ahn, Y.-W. Kim, and J. Park, Appl. Phys. Lett. **96**, 191906 (2010).
[28] S. B. Lee, S. J. Yoo, Y.-M. Kim, J.-G. Kim, and H. N. Han, Sci. Rep. **6**, 26493 (2016).
[29] S. B. Lee, S. J. Yoo, and P. A. van Aken, EPL **120**, 16002 (2017).
[30] K. L. Merkle and D. Wolf, Philos. Mag. A **65**, 513 (1992).
[31] K. L. Merkle and L. J. Thompson, Phys. Rev. Lett. **83**, 556 (1999).
[32] G. P. Pells and D. C. Phillips, J. Nucl. Mater. **80**, 207 (1979).
[33] G. P. Pells and D. C. Phillips, J. Nucl. Mater. **80**, 215 (1979).
[34] R. F. Egerton, P. Li, and M. Malac, Micron **35**, 399 (2004).
[35] S. B. Lee and Y.-M. Kim, Acta Mater. **59**, 1383 (2011).
[36] T. Malis, S. C. Cheng, and R. F. Egerton, J. Electron Microsc. Tech. **8**, 193 (1988).
[37] M. J. Hÿtch, E. Snoeck, and R. Kilaas, Ultramicroscopy **74**, 131 (1998).
[38] F. Hüe, C. L. Johnson, S. Lartigue-Korinek, G. Wang, P. R. Buseck, and M. J. Hÿtch, J. Electron Microsc. **54**, 181 (2005).
[39] P. L. Galindo, S. Kret, A. M. Sanchez, J.-Y. Laval, A. Yáñez, J. Pizarro, E. Guerrero, T. Ben, and S. I. Molina, Ultramicroscopy **107**, 1186 (2007). See Ref. [40].
[40] See Supplemental Material at http://link.aps.org/supplemental/10.1103/PhysRevMaterials.2.113405 for details of two-dimensional quadratic fitting functions; http://hremresearch.com.
[41] W. C. Mackrodt, R. J. Davey, S. N. Black, and R. Docherty, J. Cryst. Growth **80**, 441 (1987).
[42] I. Manassidis and M. J. Gillan, J. Am. Ceram. Soc. **77**, 335 (1994).
[43] J. Sun, T. Stirner, and A. Matthews, Surf. Coat. Technol. **201**, 4205 (2006).
[44] R. J. Asaro and W. A. Tiller, Metall. Trans. **3**, 1789 (1972).
[45] M. A. Grinfeld, Sov. Phys. Dokl. **31**, 831 (1986).
[46] D. J. Eaglesham and M. Cerullo, Phys. Rev. Lett. **64**, 1943 (1990).
[47] D. E. Jesson, K. M. Chen, S. J. Pennycook, T. Thundat, and R. J. Warmack, J. Electron. Mater. **26**, 1039 (1997).